Spatially distributed sensitivity of simulated global groundwater heads and flows to hydraulic conductivity, groundwater recharge and surface water body parameterization

Robert Reinecke[1], Laura Foglia[3], Steffen Mehl[5], Jonathan D. Herman[4], Alexander Wachholz[1], Tim Trautmann[1], and Petra Döll[1,2]

[1]Institute of Physical Geography, Goethe University Frankfurt, Frankfurt am Main, Germany
[2]Senckenberg Biodiversity and Climate Research Centre (BiK-F), Frankfurt am Main, Germany
[3]Department of Land, Air and Water Resources, University of California, Davis, USA
[4]Department of Civil & Environmental Engineering, University of California, Davis, USA
[5]Department of Civil Engineering, California State University, Chico, USA

Correspondence: Robert Reinecke (reinecke@em.uni-frankfurt.de)

Abstract. In global hydrological models, groundwater storages and flows are generally simulated by linear reservoir models. Recently, the first global gradient-based groundwater models were developed in order to improve the representation of groundwater-surface water interactions, capillary rise, lateral flows and human water use impacts. However, the reliability of model outputs is limited by a lack of data as well as model assumptions required due to the necessarily coarse spatial resolution.

5 The impact of data quality is presented by showing the sensitivity of a groundwater model to changes in the only available global hydraulic conductivity data-set. To better understand the sensitivity of model output to uncertain spatially distributed parameter inputs, we present the first application of a global sensitivity method for a global-scale groundwater model using nearly 2000 steady-state model runs of the global gradient-based groundwater model G^3M. By applying the Morris method in a novel domain decomposition approach that identifies global hydrological response units, spatially distributed parameter

10 sensitivities are determined for a computationally expensive model. Results indicate that globally simulated hydraulic heads are equally sensitive to hydraulic conductivity, groundwater recharge and surface water body elevation, though parameter sensitivities vary regionally. For large areas of the globe, rivers are simulated to be either losing or gaining, depending on the parameter combination, indicating a high uncertainty of simulating the direction of flow between the two compartments. Mountainous and dry regions show a high variance in simulated head due to numerical difficulties of the model, limiting the

15 reliability of computed sensitivities in these regions. This instability is likely caused by the uncertainty in surface water body elevation. We conclude that maps of spatially distributed sensitivities can help to understand complex behaviour of models that incorporate data with varying spatial uncertainties. The findings support the selection of possible calibration parameters and help to anticipate challenges for a transient coupling of the model.

1 Introduction

Global groundwater dynamics have significantly changed due to human withdrawals, and are projected to continue due to climate change (Taylor et al., 2013). Groundwater withdrawals have led to lowered water tables, decreased base flows, and groundwater depletion around the globe (Konikow, 2011; Scanlon et al., 2012; Wada et al., 2012; Döll et al., 2014; Wada, 2016). To represent groundwater-surface water body interactions, lateral and vertical flows, and human water use impacts on head dynamics, it is necessary to simulate the depth and temporal variation of the groundwater table. Global-scale hydrological models have recently moved to include these processes by implementing a gradient-based groundwater model approach (de Graaf et al., 2015; Reinecke et al., 2018). However, the lack of available input parameter data and the necessary conceptual assumptions due to the coarse spatial resolution limit the reliability of model output. These substantial uncertainties suggest an opportunity for diagnostic methods to prioritize efforts in data collection and parameter estimation.

Sensitivity analysis is a powerful tool to assess how uncertainty in model inputs affects model outcome, and can provide insights about how the interactions between parameters influence the model results (Saltelli et al., 2008). Sensitivity methods can be separated into two classes: local and global methods. Local methods compute partial derivatives of the output with respect to an input factor at a fixed point in the input space. By contrast, global methods explore the full input space, though at higher computational costs (Pianosi et al., 2016). The large number of model evaluations required can render global methods unfeasible for computationally demanding models, though increased computational resources have led to more widespread application e.g. (Herman et al., 2013b, a; Ghasemizade et al., 2017). For this reason, existing studies of global models either focus on exploring uncertainties by running their model with a limited set of different inputs for a quasi local sensitivity analysis (Wada et al., 2014; Müller Schmied et al., 2014, 2016; Koirala et al., 2018) or applying computationally inexpensive methods based on a limited set of model evaluations (Schumacher et al., 2015). For example, de Graaf et al. (2015, 2017) determined the coefficient of variation for head results in a global groundwater model with 1000 model runs evaluating the impact of varying aquifer thickness, saturated conductivity and groundwater recharge. To the knowledge of the authors, Chaney et al. (2015) is the only study of a global (land surface) model which carried out an extensive global sensitivity analysis to assess how model parameter uncertainty affects prediction of hydrologic extremes. An overview of the application of different sensitivty analysis methods for hydrological models can be found in Song et al. (2015); Pianosi et al. (2016).

We present an application of the well-established Morris method (Morris, 1991) with the **G**lobal **G**radient-based **G**roundwater **M**odel G³M (Reinecke et al., 2018). The Morris method has been successfully applied to a variety of models, ranging from hydrology (Zhan et al., 2013) to ecology models (Cariboni et al., 2007). It requires significantly fewer model runs, compared to other global methods, to provide a meaningful ranking of sensitivity parameters (Herman et al., 2013a) enabling the exploration of computationally demanding models. One drawback is that the Morris method does not provide the variance decomposition obtained with variance-based measures like Sobol (1993).

G³M uses input from, and it is intended to be coupled and integrated into, the global hydrological model WaterGAP Global Hydrology Model (WGHM) (Döll et al., 2014). This study investigates the sensitivity of steady-state hydraulic heads and

exchange flows between groundwater and surface water to variations in main model inputs (e.g. groundwater recharge and other model parameters like the riverbed conductance).

Sensitivities of the model are explored in three steps: (1) To understand the impact of improved input data, in particular hydraulic conductivity, we investigate the changes in simulated hydraulic head that result from changing the hydraulic conduc-
tivity data from the GLHYMPS 1.0 dataset (Gleeson et al., 2014) to 2.0 (Huscroft et al., 2018). (2) Based on prior experiments (de Graaf et al., 2015; Reinecke et al., 2018) eight parameters are selected for a Monte Carlo experiment to investigate sensitivities of simulated hydraulic head and groundwater-surface water interactions. The parameters are sampled with a newly developed global region-based sampling strategy and build the framework for the (3) Morris analysis. Elementary Effects (EE) are calculated and their means and variances ranked to determine global spatial distributions of parameter sensitivities and inter-
actions. The derived global maps show, for the first time, the sensitivity and parameter interactions of simulated hydraulic head and groundwater-surface water flows in the simulated steady-state global groundwater system to variations in these uncertain inputs.

2 Methodology and Data

2.1 The model G³M

G³M (Reinecke et al., 2018) is a global groundwater model intended to be coupled with WGHM (Döll et al., 2003, 2012, 2014;
Müller Schmied et al., 2014) and is based on the Open Source groundwater modelling framework G³M-f[1](Reinecke, 2018).
It computes lateral and vertical groundwater flows as well as surface water exchanges for all land areas of the globe except
Antarctica on a resolution of 5′ with two vertical layers with a thickness of 100 m. The evaluation presented in this study
is based on a steady-state variant of the model representing a quasi-natural equilibrium state, not taking into account human
interference. The stand-alone steady-state simulations were performed as initial step to identify the dominant parameters that
are also likely important for controlling transient groundwater flow.

2.1.1 Groundwater recharge

Groundwater recharge (R) is based on mean annual R computed by WaterGAP 2.2c for the period 1901-2013. Human ground-
water abstraction was not taken into account; not because it is not computed by WaterGAP but rather because there is no
meaningful way to include it into a steady-state model represents a natural equilibrium.

2.1.2 Hydraulic conductivity

Hydraulic conductivity (K) is derived from GLHYMPS 2.0 (Huscroft et al., 2018) (shown in Fig. 2 (a)). The original data was
gridded to 5′ by using an area-weighted average and used as K of the upper model layer. For the second layer, K of the first
layer is reduced by an e-folding factor f used by Fan et al. (2013) (a calibrated parameter based on terrain slope) assuming that

---

[1]Available on globalgroundwatermodel.org

conductivity decreases exponentially with depth. Conductivity of the lower layer is calculated by multiplying the upper layer value by $exp(-50mf^{-1})^{-1}$ (Fan et al., 2013, Eq. 7).

Currently only two datasets, GLHMYPS 1.0 and 2.0 (Gleeson et al., 2014; Huscroft et al., 2018), are available and are used by a number of continental and global models (de Graaf et al., 2015; Maxwell et al., 2015; Keune et al., 2016; Reinecke
5 et al., 2018). GLHMYPS 1.0 (Gleeson et al., 2014) is compiled based on the global lithology map GLiM (Hartmann and Moosdorf, 2012) and data from 92 regional groundwater models and derives permeabilities (for the first 100 m vertically) based on Gleeson et al. (2011), differentiating the sediments into the categories fine-, coarse-grained, mixed, consolidated, and unconsolidated. Permafrost regions are assigned a K value of 10^{-13} ms^{-1} based on Gruber (2012). Areas of deeply weathered laterite soil (mainly in tropical regions) are mapped as unconsolidated sediments as they dominate K (Gleeson et al., 2014).
10 The global permeability map was further improved with the development of GLHYMPS 2.0 by Huscroft et al. (2018). A two-layer set up was established in GLHYMPS 2.0 with the lower layer matching the original GLHYMPS 1.0. For the upper layer in GLHYMPS 2.0, a global database of unconsolidated sediments (Börker et al., 2018) was integrated into GLHYMPS 2.0 resulting in overall slightly increased K (Fig. 2 (a)). The thickness of the upper layer was deduced from the *depth-to-bedrock* information available from SoilGrid (Hengl et al., 2017). No thickness was assigned to the lower layer.

15 ### 2.1.3 Surface water body conductance

G^{3}M is a conceptual model with one river in every 5' grid cell. The in- and outflows are described similar to MODFLOW as flows from the cell Q, thus losing and gaining surface water bodies (lakes, wetlands and rivers) are described as

$$Q_{swb} = \begin{cases} C_{swb}(h_{swb} - h) & h > B_{swb} \\ C_{swb}(h_{swb} - B_{swb}) & h \leq B_{swb} \end{cases} \tag{1}$$

where h_{swb} is the head of the surface water body and B_{swb} the bottom elevation. The conductance C_{swb} of the surface water
20 body bed is calculated as

$$C_{swb} = \frac{KLW}{h_{swb} - B_{swb}} \tag{2}$$

where K is the hydraulic conductivity, L the length and W the width of the surface water body. For lakes (including reservoirs) C_{lak} and wetlands C_{wet}, C_{swb} is estimated based on K of the aquifer and surface water body area divided by a static thickness of 5 m. For a steady-state simulation the surface water body data shows the maximum spatial extent of wetlands, an extent
25 that is seldom reached in particular in case of wetlands in dry areas. To account for that we assume for global (surface water bodies recharged by streamflow coming from an upstream 5' grid cell) wetlands ($C_{gl.wet}$) that only eighty percent of their maximum extent is reached. For gaining rivers, conductance is quantified individually for each grid cell following an approach proposed by Miguez-Macho et al. (2007). The value of river conductance C_{riv}, according to Miguez-Macho et al. (2007), in a groundwater flow model needs to be set to such a values that, for steady-state conditions, the river is the sink for all the inflow
30 to the grid cell (R and inflow from neighbouring cells) that is not transported laterally to neighbouring cells such that

$$C_{riv} = \frac{R + Q_{eq_{lateral}}}{h_{eq} - h_{riv}} \quad h > h_{riv} \tag{3}$$

where $Q_{eq_{lateral}}$ is the lateral flow based on the equilibrium head h_{eq} of Fan et al. (2013) and h_{riv} the head of the river (E_{swb} = $h_{swb,riv}$ in Table 1). These conductance equations are inherently empirical. Future efforts will investigate using approaches appropriate for large scale models, such as described by Morel-Seytoux et al. (2017). An extensive description on the chosen equations and implications can be found in Reinecke et al. (2018).

2.1.4 Surface water body elevation

The vertical location of surface water bodies has a great impact on model outcome (Reinecke et al., 2018). Their vertical location h_{swb} is set to the 30th percentile of the $30''$ land surface elevation values of Fan et al. (2013) per $5'$ cell, e.g. the elevation that is exceeded by 70 % of the thousand $30''$ elevation values within one $5'$ cell. B_{swb} is calculated based on that head elevation with different values for wetlands and lakes (Reinecke et al., 2018, Table 1). For rivers, B_{swb} is equal to $h_{riv} - 0.349 \times Q_{bankfull}^{0.341}$ (Allen et al., 1994), where $Q_{bankfull}$ is the bankfull river discharge in the $5'$ grid cell (Verzano et al., 2012).

2.1.5 Ocean boundary

The outer boundary condition in the model is described by the ocean and uses an equation similar to MODFLOW's general head boundary condition as flow

$$Q_{ocean} = C_{oc}(h_{ocean} - h_{aq}) \tag{4}$$

where h_{ocean} is the elevation of the ocean water table set 0 m worldwide and C_{oc} the conductance of the boundary condition set to $10^{-6}m^2s^{-1}$ based on average K and aquifer thickness.

2.2 Sensitivity Analysis

2.2.1 Sensitivity of simulated head to choice in hydraulic conductivity dataset

Parameterization of aquifer properties based on hydrogeological data is an important decision in groundwater modeling. We first investigate the effect of switching to a newly available global permeability dataset to explore the sensitivity of simulated hydraulic head (h) caused by variability in geologic data. The results are then compared to the variability in parameters of the Monte Carlo experiments.

GLHYMPS 2.0 (Huscroft et al., 2018) provides an update of the only available global permeability map (Gleeson et al., 2014). To quantify how the new hydraulic conductivity estimates change the simulation outcome of the groundwater model we apply a basic sensitivity method.

$$S = \frac{\frac{h_2 - h_1}{h_1}}{\frac{K_2 - K_1}{K_1}} \tag{5}$$

where the sensitivity S of h to a change in K is calculated based on the change in h (h_1 is the hydraulic head calculated with GLHYMPS 1.0 and h_2 with GLHYMPS 2.0) and change in K_1 and K_2 the conductivity based on GLHYMPS 1.0 and 2.0, respectively.

2.2.2 Sensitivity of head and surface water body flow to choice in parameters

5   Along with K, additional parameters influence the model outcome (Sect. 2). In this study we apply the method of Morris (Morris, 1991) as a screening method to identify which parameters are most important for the two main model outcomes, namely h and groundwater-surface water interactions (Q_{swb}). The Morris method provides a compromise between accuracy and computational cost in comparison to other Monte Carlo like methods (Campolongo et al., 2007). Each model execution represents an individually randomized One Factor At a Time (OAT) experiment, where one parameter is changed per simulation. Based

10   on these model evaluation responses, the Morris method calculates Elementary Effect (EE) d for a given value of $\mathbf{X}$ for the ith model input.

$$d_i(\mathbf{X}) = \left(\frac{y(X_1, \ldots, X_{i-1}, X_i + \Delta, X_{i+1}, \ldots, X_k) - y(\mathbf{X})}{\Delta} \right) \tag{6}$$

where Δ is the trajectory step size for the parameter multiplier X_i, $\mathbf{X}$ is the vector of model parameters multipliers of size k and $y(\mathbf{X})$ the model output. The total effect of the ith parameter is computed as the mean of the EEs and is denoted as $\mu*$ (Cam-

15   polongo et al., 2007). The standard deviation of EEs (σ_i) is an aggregated measure of the intensity of the interactions of the ith parameter with the other parameters, representing the degree of non-linearity in model response to changes in the ith parameter (Morris, 1991). The derived metrics $\mu*$ and σ_i both are measures of intensity (higher values are more sensitive/interactive) and do not represent absolute values of sensitivity. Both can only be interpreted meaningfully in comparison with values derived for other parameters. To achieve that, $\mu*$ and σ_i are presented as *ranked* parameters. $\mu*$ values for all parameters are ranked

20   from highest to lowest, and the parameter with the highest value is selected as the most influential parameter. The parameter with the second highest value (*rank* 2) is the second most influential parameter and so on.

    Based on previous experiments (de Graaf et al., 2015; Reinecke et al., 2018) we identified eight uncertain model parameters presented as multipliers in Table 1. Parameter ranges were chosen to ensure that a high percentage of model realizations converge numerically. For example, the uncertainty of E_{swb} in the model is higher than the ranged used in this study, but the

25   sampling range was restricted because the parameter is especially important for model convergence. Furthermore, the chosen river conductance approach uses R as input and includes a nonlinear threshold between losing and gaining surface water bodies, which strongly affects numeric stability. As in any global sensitivity analysis, the choice of parameter ranges involves some subjectivity that may influence the ranking of sensitive parameters in the results.

2.2.3 Global hydrological response units

30   Even though the number of model evaluations are comparably less for OAT-based experiments than for All-At-a-Time (Pianosi et al., 2016), varying every parameter independently in every spatial grid cell leads to an unfeasible amount of model runs. On the other hand, the use of global multipliers that vary a parameter uniformly for all computational cells may lead to inconclusive

Table 1. Range of parameter multipliers used in the Morris experiments. Each parameter multiplier is sampled in log space ($\log_{10}(\text{Multiplier})$) with sampling based on Campolongo et al. (2007) and optimized with Ruano et al. (2012).

Parameter	P. Unit	Multiplier Range	Description
K	LT^{-1}	0.1 - 100	Saturated hydraulic conductivity
E_{swb}	L	$10^{-0.001}$ - $10^{0.001}$	SWB elevation
C_{lak}	L^2T^{-1}	0.5 - 2	Conductance of lakebed
C_{wet}	L^2T^{-1}	0.5 - 2	Conductance of wetland bed
$C_{gl.wet}$	L^2T^{-1}	0.5 - 2	Conductance of global wetland bed
C_{riv}	L^2T^{-1}	0.5 - 2	Conductance of riverbed
R	LT^{-1}	0.5 - 2	Groundwater recharge
C_{oc}	L^2T^{-1}	0.1 - 10	Conductance of the ocean boundary

C_{oc} is equal for all ocean cells

results, as the sensitivity for every cell to this change is spread to the whole computational domain. A possible solution would be to separate the globe into zones with similar geological characteristics based on the GLHYMPS dataset, but this may still result in an infeasible number of required simulations. Each simulation takes about 30 min to 1 h on a commodity computer (more if the parameters hinder a fast convergence).

5   To overcome these limitations, we introduce the use of a Global Hydrological Response Unit (GHRU). Every GHRU represents a region of similar characteristics regarding three characteristics: E_{swb} (Sect. 2.1.4), K (Sect. 2.1.2), and R (Sect. 2.1.1). This does not constitute a zoning approach often used for calibration in traditional regional groundwater modelling, only a separation into parameter multipliers. All multipliers for a given parameter for all regions are based on the same random distribution inside a given range of uncertainty for that parameter. Characteristics for each model cell are normalized to $[0, 1]$

10   and used to create a 3d point space (based on the three characteristics for each model cell). We apply a *k-means* (Lloyd, 1982) clustering algorithm to identify these regions.

K-means clustering partitions n points into k clusters where each point belongs to the cluster with a minimized pairwise squared distance to the mean in a cluster. Figure 1 (a) shows a map of k-means clustering (6 clusters) categories based on normalized three-dimensional space of E_{swb}, K, and R per grid cell.

15   The number of clusters was determined based on the feasible number of model evaluations. *k-means* constitutes an unsupervised machine learning approach that builds the required number of clusters automatically, thus it is necessary afterwards to examine what main characteristics these clusters represent (shown in Table 2). Characteristics are encoded as relative values (high ($\uparrow$), medium ($\sim$), low ($\downarrow$)) of the three input values based on their mean value per cluster. These characteristics are used to connect calculated parameter sensitivities to GHRUs when analyzing the results of the experiment.
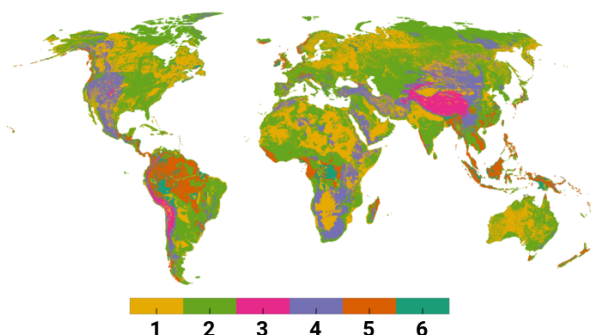
Figure 1. Map of k-means clustering categories each representing a GHRU (a). Each color identifies a region where the combination of all three parameters is similar.

Table 2. Mean values of GHRU characteristics and their summarized description, where $\uparrow$ is read as a relatively high value, $\sim$ as medium, and $\downarrow$ as low; e.g. $\uparrow\uparrow$ E indicates a cluster with very high and relatively high ($\uparrow$) average E_{swb}. Additionally, the last two columns show the percentage of cells per GHRU where $\mu*$ of h and Q_{swb} could be reliably determined (described in Sec. 3.2.6).

					% of reliable $\mu*$	
GHRU	$\mu(E_{swb})$[m]	$\mu(K)$[m/day]	$\mu(R)$[mm/day]	GHRU description	h	Q_{swb}
1	454	10^{-4}	0.15	$\sim$ E, $\uparrow$ K, $\sim$ R	9.54 %	6.58 %
2	286	10^{-6}	0.15	$\downarrow$ E, $\sim$ K, $\sim$ R	12.07 %	14.41 %
3	4107	10^{-6}	0.13	$\uparrow\uparrow$ E, $\sim$ K, $\downarrow$ R	0.08 %	4.09 %
4	1355	10^{-6}	0.11	$\uparrow$ E, $\sim$ K, $\downarrow$ R	3.17 %	17.19 %
5	303	10^{-6}	1.24	$\downarrow$ E, $\sim$ K, $\uparrow$ R	31.62 %	26.37 %
6	194	10^{-4}	1.25	$\downarrow$ E, $\uparrow$ K, $\uparrow$ R	29.00 %	14.36 %

2.2.4 Experiment Configuration

With seven parameters per GHRU plus the ocean boundary, 10 000 base points were sampled in total (Campolongo et al., 2007) and optimized using Ruano et al. (2012). The experiment resulted in 1848 simulations with an overall runtime of two months on a machine with 20 computational cores (enabled hyper-threading) and 188 GB RAM. Each simulation required about 8 GB

5 of RAM and was assigned four computational threads while running the simulations in cohorts of 10 simulations at once. Each simulation was an OAT experiment (an extended explanation of OAT and other sensitivity experiment setups and methods can be found in Pianosi et al. (2016)). Changes in parameters were stacked over all experiments. Thus, an experiment may have changed R (also affecting C_{riv} for gaining conditions) while containing a C_{riv} multiplier from a previous experiment. Sampling and analysis was implemented with the Python library *SALib* (Herman and Usher, 2017). For each experiment,

10 the model was run until it reached an equilibrium state (steady-state model). All other parameters and convergence criteria can be found in Reinecke et al. (2018). If a simulation failed (6 of 1848 did not converge) the missing results were substituted

randomly from another simulation within the cohort to preserve the required ordering of parameter samples for the used Python implementation of Morris. This number is low enough that it does not bias the results in any significant way (Branger et al., 2015).

A converged simulation does not necessarily constitute a valid result for all computed cells. Numeric difficulties based on

5   the model configuration (due to the selected parameter multipliers) may lead to cells with calculated h that are unreasonable. Confidence intervals (95 %) are derived via bootstrapping using 1000 bootstrap resamples, following Archer et al. (1997).

3   Results

3.1   Sensitivity to updated GLHMYPS dataset

Global-scale hydrogeological data is limited. Figure 2 (b) shows the change in K between GLHYMPS 1.0 (Gleeson et al.,

10   2014) and the upper layer of GLHYMPS 2.0 (Huscroft et al., 2018) where an overall increase can be observed due to the change in unconsolidated sediments. Although unconsolidated sediments cover roughly 50 % of the world's terrestrial surface, their extent was underestimated in previous lithologic maps by half (Börker et al., 2018). The largest increase of K can be found between 50 and 70 °N because of glacial sediments that were assigned high K values. Different lithologies, e.g. alluvial terrace sediments and glacial tills, have all been grouped into the hydrolithological category of sand. Areas of decreased

15   conductivity are e.g. the Great Lakes, south of Hudson Bay, and parts of Somalia. The area around Hudson Bay was assumed to consist of unconsolidated sediments in GLHYMPS 1.0 (Gleeson et al., 2014) and was changed to consolidated. In Somalia, evaporites, which are known for low K, were incorporated from the Global Unconsolidated Sediments Map Database (GUM) (Börker et al., 2018). Furthermore, GUM provides a detailed mapping of loess and loess-like depositions, which were assigned lower K values. These regions can be observed to be the only regions with reduced K (Fig. 2 (b)). Overall, the increase in

20   unconsolidated sediments is probably the main cause for the increased K.

Due to the change in K, the simulated h changes accordingly (Fig. 2(c)). In areas where the K decreased h increased e.g. eastern North America. Overall heads decreased, especially in central Russia by up to 10 to 100 m. A slight increase in head can be observed in areas with no change in K. This can be either due to changes in groundwater flow patterns due to the overall increase in K or due to numerical noise.

25   Based on these results, a local sensitivity index was calculated using Eq. (5), shown in Fig. 2 (d). White constitutes areas where either the relative change of K was zero or the head of the GLHYMPS 1.0 simulation was zero. Areas with a sensitivity index below (-)0.1 probably constitute variations that can be accounted to numerical differences in simulation outcome. Overall, h and K change in the opposite directions (positive values indicate a change into the same direction). An overall increase in K has led to a overall decrease in h as the higher K values are able to transport more water for a given hydraulic gradient,

30   especially along coastlines and mountainous areas. Increased sensitivity indexes can be observed at boundaries of large areas where K changed, whereas the h changes inside that area are relatively small (e.g. Arabian Peninsula). In regions where an increase in K leads to a decrease in head, an increase of h at the boundary to other hydrolithological structures can be observed. Areas with changing indexes next to each other, e.g. in the Sahara, possibly point to a numerically unstable model region with
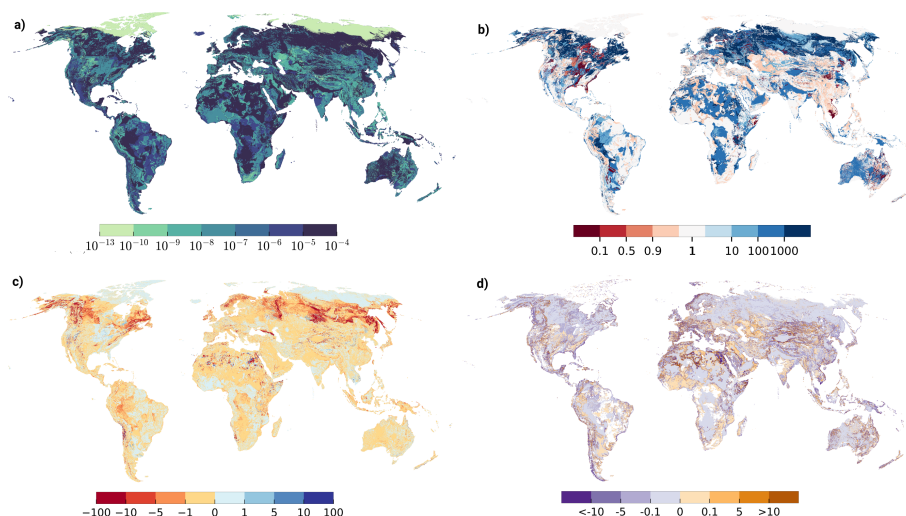
Figure 2. Impact of hydraulic conductivity datasets GLHYMPS 1.0 and GLHYMPS 2.0. (a) GLHYMPS 2.0 [ms^{-1}], (b) K differences, expressed as K(GLHYMPS 2.0)/K(GLHYMPS 1.0). Blue indicates higher values in GLHYMPS 2.0. (c) h(GLHYMPS 2.0) minus h(GLHYMPS 1.0) [m], (d) the sensitivity of h to change in the GLHYMPS dataset based on Eq. (5) (white indicates that no index could be calculated).

a general sensitivity to parameter changes. GLHYMPS 2.0 represents the best available global data for hydraulic conductivity, and the results of this initial experiment indicate a significant sensitivity to updating the model with this new dataset.

3.2 Monte Carlo experiments

To assess the variability of model outputs we used the Monte Carlo-like OAT experiments to analyze the outcomes of 1848
5   model realizations.

3.2.1 Variability of hydraulic head

The spatial distribution of variability in the main model output h provides insights into model stability and highlights regions which are most sensitive to parameter changes. Observable differences between simulations can be caused by: (1) the parameter change of the OAT experiment, (2) the interactive effects due to combinations of parameter changes, (3) numerical noise (slight
10   variations in outcome due to the nature of the numerical algorithm or floating point errors that cannot be attributed to a specific parameter change), and (4) a non-optimal solution of the groundwater equation even if the convergence criterion is met. The latter error can be observed in regions of the model where a strong non-linear relation may produce solutions that fit the convergence criterion but should be considered non-valid, e.g., because of a mass-balance that is not in an acceptably precise.

    Figure 3 shows the absolute coefficient of variation (ACV) of h per cell over all Monte Carlo experiments. The ACV is
15   used to make a sound comparison of variance taking into account the mean of the h value per cell (because the mean might
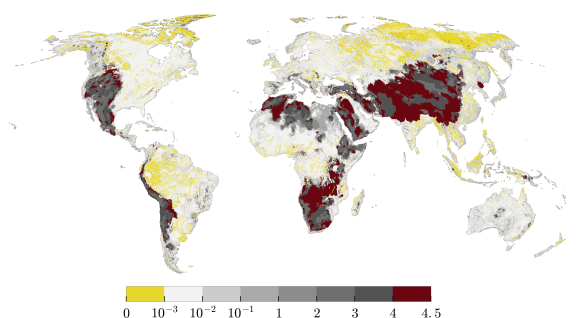
Figure 3. Absolute coefficient of variation $(\sigma(h)\mu(|h|)^{-1})$ [%] of simulated h per cell over all Monte Carlo realizations. Yellow indicates that h results changed very little, white to gray values indicate a growing difference in model results, and red values indicate a very high variation of h over all model realizations.

be negative the absolute value is used). Yellow indicates that h changed little (mostly for regions with shallow groundwater), white to gray values indicate a growing difference in model results, and red values indicate a high variation of h over all model realizations. The latter areas represent either very low R (Sahara, Australia, South Africa) or a high variance in elevations, e.g., Himalaya, Andes and the Rocky Mountains. These are expected to have a high sensitivity to parameter changes as the

5   multiplier of E_{swb} produces the highest shifts in regions with high elevation that might cause a switch from gaining to losing conditions and vice versa (discussed in Sect. 3.2.2). Additionally, a change in R directly influences the conductance term C_{riv} that might also be changed by a multiplier. These combinations may yield conditions that are exceptionally challenging for the numerical solver.

     Areas with a high variance in results will also produce wide confidence intervals and are highlighted in Fig. A2.

10   Figure 4 relates the uncertainty in h, due to a change from GLHYMPS 1.0 to 2.0 to the interquartile range of h of all Monte Carlo realizations, thus uncertainty in h due to parameter variation. Parameter variation is the dominant cause for h variability in mountainous regions, whereas the change in geologic data has a dominant impact in northern latitudes and the upper Amazon. In Australia, central Africa, and northern India the impact of increasing K is almost as high as the variability caused by the variation of parameters in the Monte Carlo experiments. This suggests that a reduced uncertainty in K in these

15   regions will improve the model results.

3.2.2 Variability of losing/gaining surface water bodies

Surface water bodies that provide focused, indirect groundwater recharge to the aquifer system are an important recharge mechanism to support ecosystems alongside streams (Stonestrom, 2007). Especially in arid regions, they are important for agriculture and industrial development.

20   Losing or gaining surface water bodies are determined by h in relation to E_{swb}. Figure 5 shows for each grid cell the percentage of the model runs in which the the surface water bodies in the cell lose water to the groundwater. Regions with a higher percentage are regions that are in losing conditions independent of the applied parameter changes. Areas with the
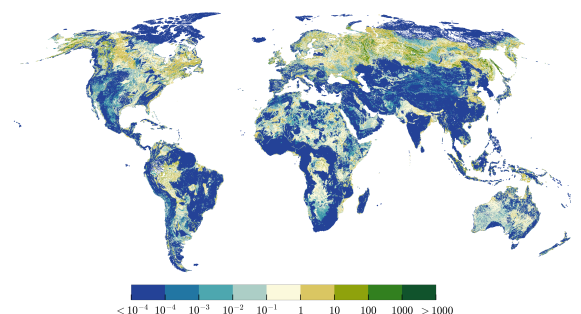
Figure 4. Uncertainty in h caused by variability in geologic structure (dominant in blue to light blue) in relation to uncertainty in h caused by variability in parameters based on Monte Carlo simulations (dominant in brown to green) calculated as $\frac{|h1-h2|}{\mathrm{IQR}(h_{mc})}$ where $h1/2$ is the simulated head based on GLHMYPS 1.0 and 2.0 and h_{mc} the simulated head of all Monte Carlo experiments.
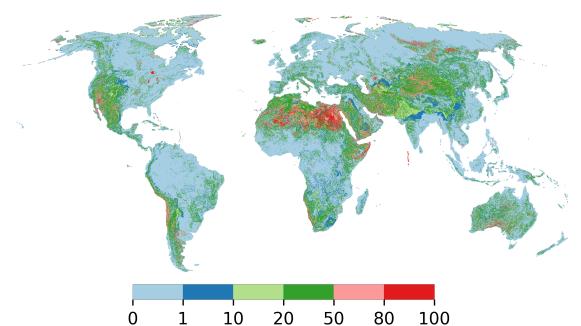
Figure 5. Percentage of all Monte Carlo realizations that resulted in a losing surface water body in a specific cell.

highest deviation in h (Fig. 3), thus the lowest agreement over all model realizations, are similar to the regions where some parameter combinations lead to losing surface water bodies, while others lead to gaining surface water bodies (Fig. 5). Overall arid and mountainous regions show high percentages of Monte Carlo realizations with losing conditions, with dominantly 20-50 % of the realizations resulting in losing surface water bodies. h in these regions falls below E_{swb} either due to low recharge or high gradients. Surface water-groundwater interaction in these regions should be more closely investigated to improve model performance. The Sahara region stands out with large areas that contain losing surface water bodies in almost all model realizations. Values close to 100 % are furthermore reached in the Great-Lakes, the Colorado Delta, the Andes, the Namib Desert, along the coast of Somalia, the Aral lake, lakes and wetlands in northern Siberia, and partially in Australian wetlands. Wetlands in Australia and the Sahara are likely to be overestimated in size in the context of a steady-state model.

3.2.3 Parameter sensitivities as determined by the method of Morris

The global-scale sensitivity of h and Q_{swb} is summarized in Table 3 that lists the percentage fractions of all cells for which a certain parameter has a certain rank regarding sensitivity and parameter interaction.

Overall, E_{swb} and R are the most important parameters for both model outputs over all ranks, followed by K. Q_{swb} is more sensitive to R than h, whereas h is more sensitive to E_{swb}. C_{riv} appears only dominant in the second and third rank for both model outputs. This means that for the majority of cells a change in E_{swb} and R, rather than C_{riv} dominates changes in Q_{swb} and h. K and R directly influence the calculation of C_{riv} and thus show a higher sensitivity.

The standard deviation of EEs (σ_i) is an aggregated measure of the intensity of the interactions of the ith parameter with the other parameters, representing the degree of non-linearity in the model response to changes in the ith parameter Morris (1991). A high parameter interaction indicates that the total output variance rises due to the interaction of the parameter with other parameters.

E_{swb} shows higher interactions for h than for Q_{swb}. C_{riv} shows a high interaction on the first rank even if it is not the dominant effect. This interaction is likely due to changes and K and R that directly influence the computation of C_{riv}. Both model outputs are sensitive to changes in R but show a relatively low degree of interaction for the first rank. A higher percentage of cells with an increased interaction of R is only visible in the second and third rank.

Lakes and wetlands show low sensitivity and interaction in relation to total number of cells in Table 3 because they only exist in a certain percentage of cells. Table 4 shows the percentage fractions relative for cells with more than 25 % coverage of a lakes, global wetlands, and/or wetlands. The dominant parameter (by percentage) for all cells with respective surface water body is always E_{swb} for h (in 79.2 % of the lakes and in (79.9 %) 66.3 % of the (global)wetlands) and R (~54-77 % of all cells) for Q_{swb}. For the second rank the conductance of the surface water body $C_{lak,wet,gl.wet}$ dominated h, C_{riv} for Q_{swb}. Thus for lakes and wetlands E_{swb} and R are more relevant to h and Q_{swb} than the conductance of these surface water bodies.

3.2.4 Maps of global sensitivity

To show the spatial distribution of the parameters that affect h and Q_{swb} the most, ranked parameters were plotted for every cell in Fig. 6. The top of Fig. 6 represents the most sensitive parameters in terms of h (left) and Q_{swb} (right). Areas that should be judged with caution due to overlapping CIs are shown in Fig. A2.

E_{swb} stands out for mountainous regions and regions with low recharge aligned with regions in Fig. 3 and Fig. A3 with spots of C_{riv}. E_{swb} is dominant for Q_{swb} e.g. Rocky Mountains, Andes, Hijaz Mountains in Saudi Arabia and the Himalaya. R stands out in regions in the Tropical Convergence Zone with large R and in northern latitudes for Q_{swb}. K seems to be equally spatially distributed for h as well as for Q_{swb}. It is most important for h in Australia, the northern Sahara, the Emirates, and across Europe. There seems to be no correlation between the initial K spatial distribution and a highly ranked K sensitivity. Areas with a dominant K are possibly influenced by a high interaction with other model components (K shows a high interaction Table 3 that is also reflected spatially in Sect. 3.2.5). E_{swb} stands out in the Sahara where likely overestimated

Table 3. Percentage fractions of simulated cells with parameter sensitivity $\mu*$ and parameter interaction σ per model output h and Q_{swb}, where the respective output is most sensitive to the listed parameter. For example h is the most sensitive to E_{swb} (Rank 1) in 57.2% of all grid cells, while K is the second most important parameter for h in 24.2% of those cells. Fractions are shown for the first three ranks.

| | | % of cells | | | | | |
| | | Rank 1 | | Rank 2 | | Rank 3 | |
Para.	Output	$\mu*$	σ	$\mu*$	σ	$\mu*$	σ
K	h	24.2	18.8	21.7	12.9	7.1	4.3
	Q_{swb}	18.4	15.4	21.1	7.3	8.8	4.7
E_{swb}	h	57.2	46.3	14.8	19.9	13.4	18.9
	Q_{swb}	18.5	14.3	11.2	27.7	36.0	34.4
C_{lak}	h	1.0	0.5	3.9	2.4	4.3	2.5
	Q_{swb}	0.5	0.6	2.2	0.9	2	0.9
C_{wet}	h	1.4	0.5	3.4	1.4	5.3	4.5
	Q_{swb}	0.5	0.8	3.6	2.1	4.2	2.8
$C_{gl.wet}$	h	0.9	0.9	1.8	10.2	8.4	8.1
	Q_{swb}	0.4	0.8	2.3	15.2	9.4	7.8
C_{riv}	h	2.0	28.0	32.8	29.3	28.7	18.1
	Q_{swb}	1.4	62.6	47.8	16.2	28.8	10.0
R	h	13.4	4.1	22.7	23.6	33.8	43.2
	Q_{swb}	59.8	5.1	11.3	30.5	10.7	39.2
C_{oc}	h	1.3	1.0	0.3	0.2	0.5	0.4
	Q_{swb}	0.5	0.4	0.5	0.2	0.2	0.2

Percentage of cells with reliable (overlapping CIs discussed in App. 1 and Sect. 3.2.6)
$\mu*$: 11.8 % (h) and 13.3 % (Q_{swb}).

wetland extents (Reinecke et al., 2018) have a high impact on h. Q_{swb} seems to be more robust to show the effects in the highly variable regions and indicates the assumption that E_{swb} is also mainly responsible for the h variations observed in Sect. 3.2.1.

The second rank (second row in Fig. 6) shows values that are not as important as the top row but dominant over all other parameters. In the highly variable regions K and for parts of the Himalaya R are dominant in the second rank. The C_{wet} appears as dominant parameter in areas with large wetlands with a bigger impact on Q_{swb} results than on h. C_{lak} is clearly visible in parts of Nepal and along the Brahmaputra. In the Tropical Convergence Zone C_{riv} and K dominate for Q_{swb}, whereas results for h show a mix of $C_{gl.wet}$ C_{wet} and C_{riv}.

Zooming in on Europe (Fig. 7) for h, as an example, shows a similar trend to the global picture that R and K have the highest impact on h along with E_{swb}. E_{swb} is dominant in mountainous regions like the Alps and the Apennines as well in regions with lots of surface water bodies e.g. southern part of Sweden in the area of lake Vättern and Vänern and in the Finnish Lakeland. R appears dominant in east Italy in the lagoon of Venice and Marano, the Netherlands, and the wetlands in southwestern France.

Table 4. Percentage fractions of the most frequent parameter for rank 1 and 2 of all cells with with more than 25 % coverage of a lakes, global wetland, or wetland.

	$\mu*(h)$		$\mu*(Q_{swb})$	
	% R. 1=E_{swb}	% R. 2=$C_{lak,wet,gl.wet}$	% R. 1=R	% R. 2=C_{riv}
Lakes	79.2	64.6	54.2	38.8
Wetlands	66.3	47.3	77.2	46.9
Gl. Wetlands	79.9	56.4	66.3	[1]31.7

[1] C_{riv}=31.7 %, $C_{gl.wet}$=40.6 %.

Percentage of second most frequent parameter not shown. Percentage in relation to cells with lakes, global wetland, or wetland > 25 %. Percentage-wise R. 1($\mu*(h)$) was always followed by R except for global wetlands were the second most frequent R. 1 was $C_{gl.wet}$. R. 1($\mu*(Q_{swb})$) was followed percentage-wise by E_{swb} except for local wetlands with K, R. 2($\mu*(Q_{swb})$) by $C_{lak,wet,gl.wet}$ except for global wetlands with C_{riv}.
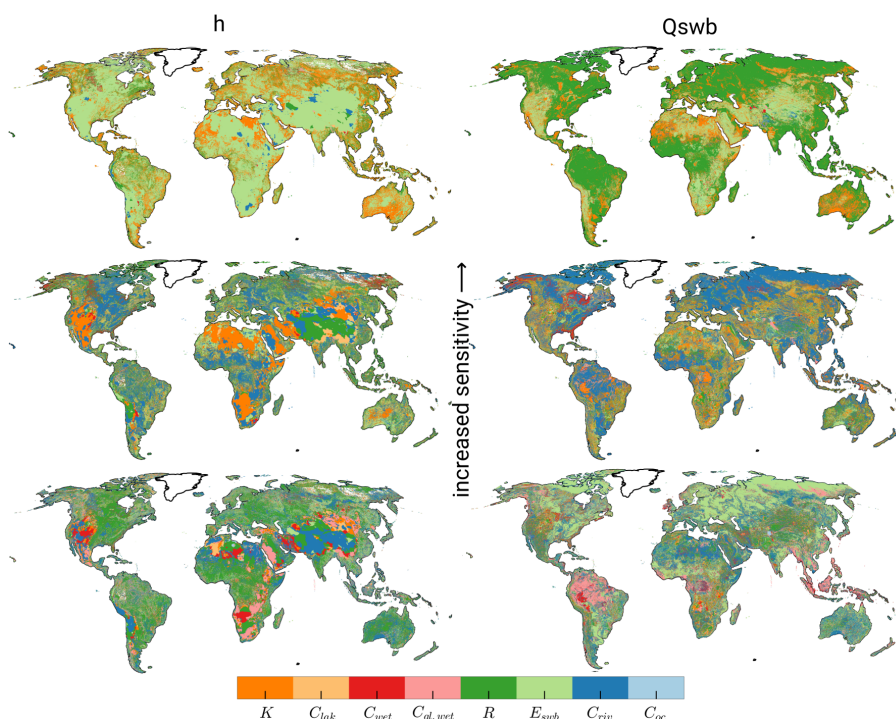
Figure 6. Ranking of parameter sensitivity of h (left) and Q_{swb} (right). Parameters are ranked from top to bottom by $\mu*$ values.

Almost invisible in the global picture is C_{oc}, a dominant parameter for most cells that have the ocean as boundary condition (only observable for h). Predominantly C_{riv} follows E_{swb} as second most important parameter. Only visible in the second rank are the wetlands e.g. in west Scotland.
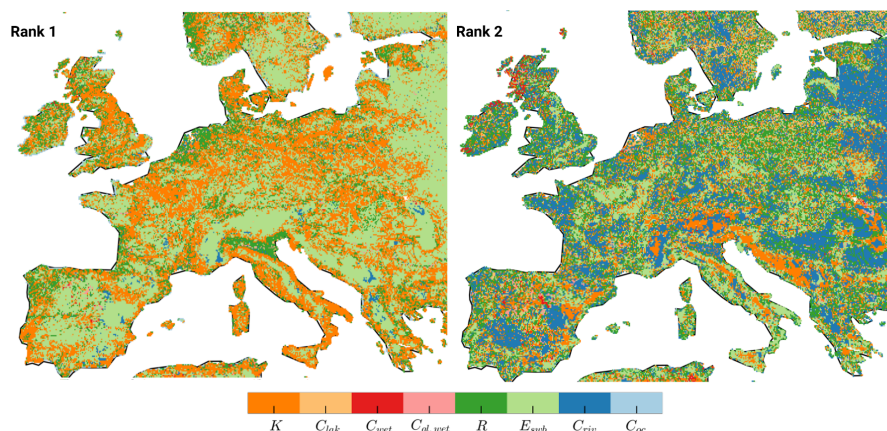
Figure 7. Zoom in of Europe of Fig. 6. Ranking of parameter sensitivity of h (left: rank 1, right: rank 2).

3.2.5 Maps of global parameter interaction

Similar to the spatial parameter sensitivities Fig. 8 shows the parameter interactions for h and Q_{swb}. Parallel to Fig. 6, the first row of Fig. 8 represents the most interactive parameters in terms of h change (left) and Q_{swb} (right). The highest interaction with other parameters can be observed for E_{swb} for regions with high h variability similar to Fig. 6. C_{riv} shows a high

5 interaction in regions sensitive to R (compare Fig. 6) and is more visible for Q_{swb}.

K regions in the second rank are similar to where K already showed a high sensitivity for h (compare Fig. 6). In the Himalaya R and C_{riv} show a large spatial pattern. For Q_{swb}, $C_{gl.wet}$ is clearly visible where C_{riv} was most interactive before.

3.2.6 Sensitivity per GHRU

10 Average sensitivities and parameter interactions for each of the six GHRUs are shown in Fig. 9 (a). A dominant average per GHRU does not imply a rank 1 in each cell but rather provides an indication of its average importance per GHRU. Each GHRU is described by the notation in Table 2. The shown average sensitivities and interactions are normalized to [0,1] because the calculated $\mu*$ and σ present no absolute measure of sensitivity. Mean values of $\mu*$ and σ that are very close to zero are not shown in Fig. 9.

15 The values shown in Fig. 9 (a) should be judged with caution as they also include the regions Fig. A2 shown to be unreliable. To judge the reliability of the outcomes per GHRU Table 2 shows the percentage of reliable results for h and Q_{swb} for each GHRU, where reliable results exclude over 80% of all sensitivity values because their CI overlapped (compare Fig. A2 and explanation Fig. A1). Figure 9 (b) shows only cells with reliable results, based on their confidence intervals, resulting in 11.8 % of all grid cells for h and 13.3 % for Q_{swb}. GHRUs in high and very high elevations show low reliability concerning h results

20 as expected (compare Fig. 3). Q_{swb} appears as more robust in these regions.
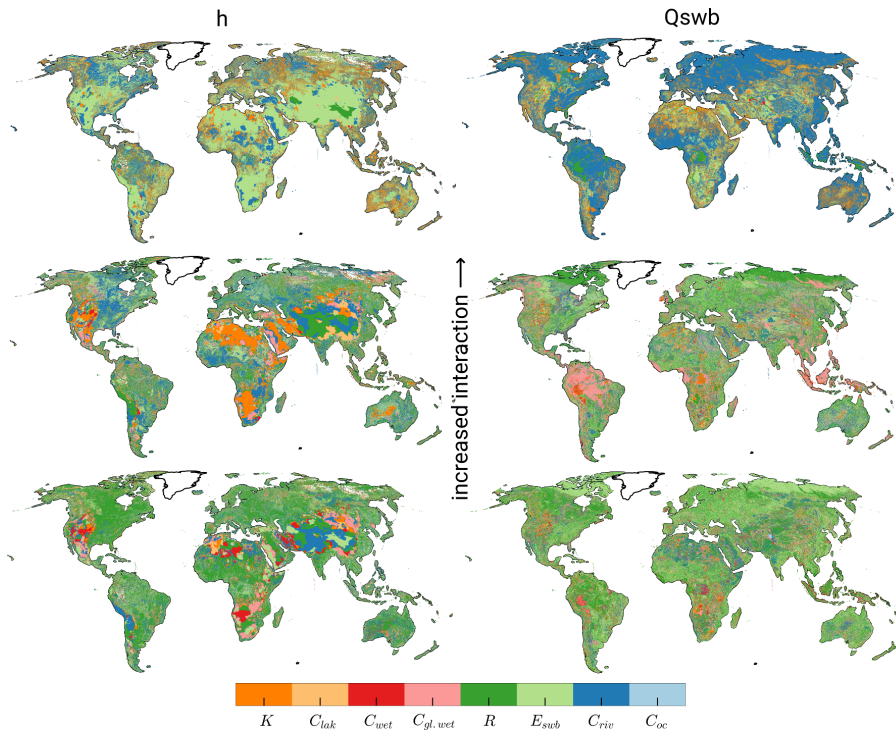
Figure 8. Ranking of parameters interaction (σ of EE is an indicator for parameter interaction) based on h (left) and Q_{swb} (right). Parameters are ranked from top to bottom by Σ values.

Figure 9 (a) shows a similar picture to the two global maps (Fig. 6, 8). All GHRUs show a linear correlation of sensitivity and degree of interaction. The GHRU with average elevation, average recharge, and high K (GHRU 1) shows higher average response in Q_{swb} than h. h as most sensitive to C_{riv}, and less sensitive to the other parameters. Q_{swb} is clearly most sensitive to K and $C_{gl.wet}$ and shows a high interaction in this GHRU. Lower-lying regions with average K and R (GHRU 2) show

5   high sensitivity of h only to E_{swb} with a high interaction while Q_{swb} is affected in decreasing order by $C_{gl.wet}$ and K. Results for h sensitivity in GHRU 3, with very high elevations, average K and low R, should be judged with caution because only a very low fraction is based on results with non-overlapping CIs (Table 2). Compared to other GHRUs, 3 shows rather clustered sensitivities and parameter interactions. h is most sensitive to E_{swb} and R and Q_{swb} to C_{lak}, K, and C_{wet}. GHRU 4, which differs from GHRU 3 by its high but not very high land surface elevation, shows E_{swb}, K, and R as clearly most dominant and

10   interactive parameter for Q_{swb}, followed by C_{wet}. Similar Q_{swb} is most sensitive to E_{swb} and K. In low-lying and rather flat regions with high groundwater recharge (GHRU 5), sensitivities of h are close to zero except for K possibly because changes in h are to small in flat regions (compare Fig. 3) due to small h gradients. Q_{swb} is most sensitive to E_{swb} and $C_{gl.wet}$. GHRU 6 is relatively small and like GHRU 5 only occurs in the tropical zone (Fig. 1 (a)). In this GHRU, which differs from GHRU 5 only by K being high instead of average, the dominant parameters of Q_{swb} are similar to other GHRUs where E_{swb} is clearly

15   the most dominant followed by R and K. h shows a response to wetlands but again like in 5 a very low response to E_{swb}.

Taking into account only the reliable regions changes the perception in Fig. 9 (b). GHRU 1 shows rather similar sensitivities and parameter interactions as compared to other GHRUs. h is most sensitive to E_{swb}, and only somewhat less sensitive to C_{riv} and C_{wet}. Q_{swb} is clearly most sensitive to C_{riv} and shows a high interaction in this GHRU. GHRU 2 shows high sensitivity of h only to E_{swb} with a high interaction while Q_{swb} is equally affected by K, E_{swb} and R. Results for h sensitivity in GHRU

5   3 are not very representative for the whole GHRU as only a very small fraction of cells shows reliable results (Table 2). Like in GHRU 2, Q_{swb} is equally affected by by K, E_{swb} and R. GHRU 4 shows E_{swb} as clearly most dominant and interactive parameter for h, followed by K and C_{wet}. For GHRU 5, sensitivities of h could not be determined reliably possibly because changes in h are to small in flat regions (compare Fig. 3) due to small h gradients. Q_{swb} is most sensitive to R (as rivers are gaining rivers that need to drain groundwater recharge) followed by K. In GHRU 6 the dominant parameters of Q_{swb} are the

10   same as for GHRU 5 (except for E_{swb}) while h is most sensitive to C_{lak}.

4   Discussion

This study presents a novel spatially distributed sensitivity analysis for a high-resolution global gradient-based groundwater model encompassing 4.3 million grid cells. While these maps are challenging to interpret, they yield new ways of understanding model behavior and can help to focus efforts in collecting observation data for specific regions for future calibration. However,

15   the large number of grid cells with either zero sensitivity values or unreliable results limit the relevance and applicability of the study results. The study suggests that the highly non-linear and conceptual approach to the surface water body conductance (in particular the sudden change of conductance between gaining and losing rivers) needs to be revised as it may affect the stability of transient model results. Additionally the results suggest that elevation of the water table of surface water bodies is a promising calibration parameter alongside with hydraulic conductivity.

20   The presented results need to be considered against the backdrop of the high h variability of the Monte Carlo experiments (Sect. 3.2.1). Some of these simulations cannot be considered as a valid result for a h distribution. This is due to multiple model challenges: (1) the evaluated model is a numerical model and thus behaves differently for different parameterizations, (2) the equations used for rivers present a non-linear model component (switch between equations for gaining and losing conditions as well as relation to K and R), (3) the convergence criterion for the steady-state solution is solely based on a vector norm of

25   residuals and maximum h change between iterations and do not contain an automated check for a reasonable mass balance. On the other hand, it is challenging to include a validation mechanism in the presented analysis to alleviate these problems while maintaining a reasonable model runtime (as a stricter convergence criterion will most likely increase the number of necessary iterations) and/or number of necessary model runs. It is questionable whether results based on different convergence criteria can be compared. This would necessitate including the numeric stability in the sensitivity analysis as well.

30   Around 30 % of all $\mu*$ values had a confidence interval that was larger than 10 % of the $\mu*$ value. This suggests that even more model runs are required and that large extents of the model experienced numerically unstable results as the spatial distribution of head variance and large confidence intervals overlap.
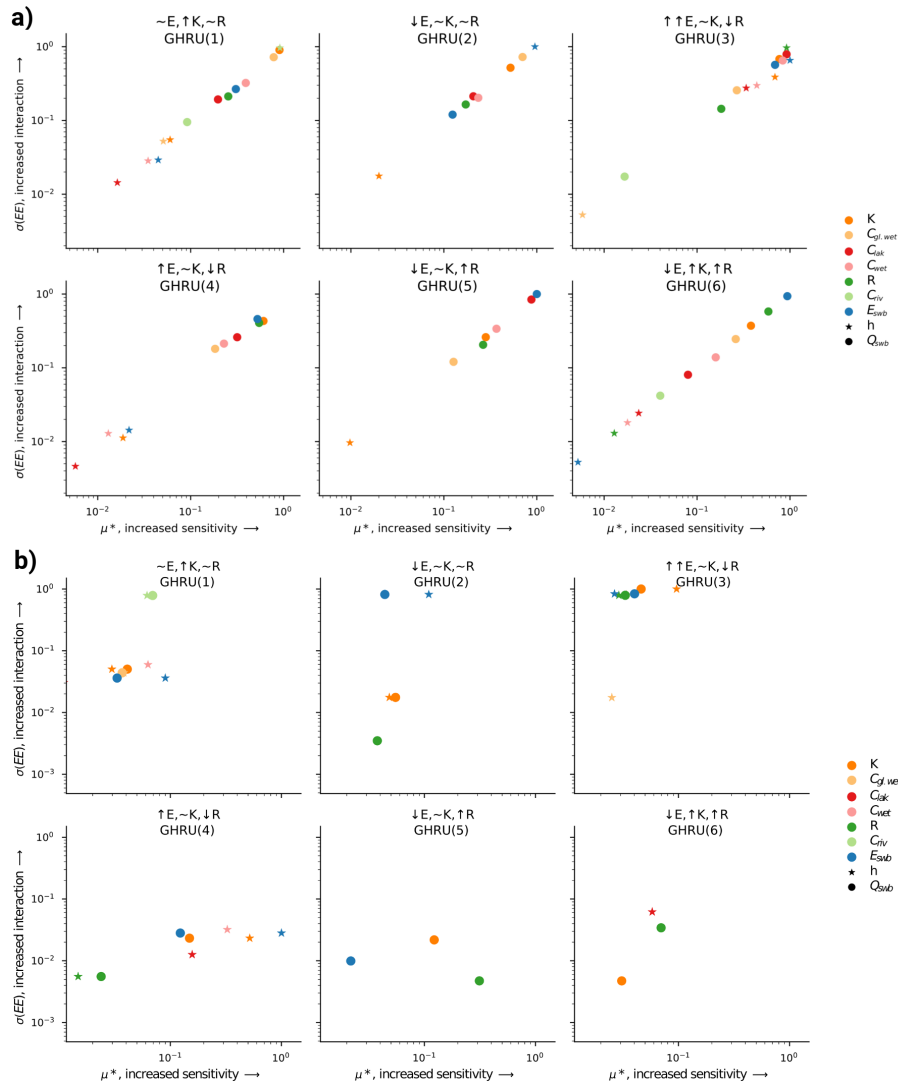
Figure 9. Normalized average sensitivity and parameter interaction per GHRU for h and Q_{swb} (a). If a parameter is not present the mean sensitivity for that GHRU was close to zero. Does not include ocean parameter sensitivity. Mean characteristics, their symbols for each GHRU, and the reliability of the sensitivity measure (only $\mu*$ not σ) are shown in Table 2. (b) Only reliable results (after removing overlapping CI).

The selection of parameter ranges can influence the results of a sensitivity analysis significantly (Pianosi et al., 2016). Even parameters that are suspected of not being sensitive can show highly nonlinear behavior in certain parts of the parameter space that are only activated when one expands the ranges of the parameters. The presented ranges in this study do not explore the full assumed uncertainty range. Specifically, the small range of E_{swb} is likely influencing the outcome of the parameter rankings.
5   The range was chosen to allow a reasonable number of simulations to converge as the range of E_{swb} directly influences the numerical stability of the model. The presented results, however, do show that the model output is highly sensitive to changes

in E_{swb} in most areas of the globe. The response in mountainous regions can be attributed to applying E_{swb} as a multiplier, which has a higher impact in regions where the initial water body elevation is high. On the other hand, this is accounting for the fact that the uncertainty of E_{swb} is largest in regions with highly variable topography per 5' grid cell.

5   The only previous sensitivity analysis of a global gradient-based groundwater model to out knowledge was done by de Graaf et al. (2015). Based on varying K, aquifer thickness, and R, the coefficient of variation of the steady-state hydraulic head was computed (de Graaf et al., 2015, Fig. 5). From that analysis it was determined that K has the highest impact and aquifer thickness the lowest. It is not clear how the coefficient of variation determined these outcomes. The relatively low impact of aquifer thickness was observed also by Reinecke et al. (2018). Therefore, this parameter was not included in this study. Both de Graaf et al. (2015) and this study show a high h variance in parts of Australia and the Sahara (de Graaf et al., 2015, Fig. 5)
10 possibly due to the low initial R. Variations in the mountainous regions, on the other hand, are not reflected in de Graaf et al. (2015) as their analysis did not vary E_{swb}.

    Besides the large h variance, which is likely the main cause for the low percentage of reliable cells, the confidence intervals of the sensitivity indices in this experiment suggest that additional simulations are necessary to determine more reliable results. Additionally, the small parameter ranges, required for stable model runs, influenced the overall outcome and might be a reason
15 for cells with inconclusive results.

    For cells with lakes and wetlands, E_{swb} dominates over the variations in conductance for h (Table 4), confirming the importance in determining the surface water body elevation. For Q_{swb}, on the other hand, R is most influential in these cells even though it does not affect the conductance equation for these surface water bodies. Apparently, available recharge is driving the interaction more than it influences changes in head. In regions with high recharge (GHRU 5) Q_{swb} was more robust to param-
20 eter changes than h. This is possibly due to the generally lower response in Q_{swb} to changes in E_{swb}, which can be explained by the constant flow for losing surface water bodies (incl. rivers) as soon as h drops below E_{swb}. Thus changes is E_{swb} do not affect Q_{swb} afterwards (as long as the surface water body remains in losing conditions). Both model outcomes show a high sensitivity to R while the interaction of R is only visible at the 3rd rank suggesting that if R changes other parameter changes do not influence the model response further.

25   Separating the complex global domain into a selected number of GHRUs enables a sensitivity analysis in accordance with computational constraints (e.g. maximum number of core hours). It alleviates the drawbacks of global-scale multipliers while keeping a reasonable number of total simulations. The presented decomposition based on three parameters E_{swb}, K, and R was guided by the high sensitivity of model output to these parameters. Other factors like lithology and surface water body characteristics should be investigated as additional characteristics for GHRUs.

30   5   Conclusions

For the first time, spatially distributed sensitivities of the global steady-state distribution of hydraulic head and flows between the groundwater and the surface water bodies were calculated and presented. We found the Morris sensitivity analysis method can yield insights for computationally challenging (concerning computation time and numerical difficulties) models

with reasonable computational demand. This study applied a novel approach for domain decomposition into GHRUs. Applying parameter multipliers simultaneously to all grid cells within each of the six GHRUs allowed a more meaningful sensitivity calculation, than it would be possible if the parameters would have varied simultaneously in all grid cells, while maintaining a feasible the number of simulations.

5   Based on only a small fraction of grid cells for which parameters could be ranked reliably according to their importance for simulated model output, steady-state hydraulic heads (h) were found to be comparably affected by hydraulic conductivity (K), groundwater recharge (R) and the elevation of the water table of surface water bodies (E_{swb}). Rankings for individual grid cells varies, but globally none of the three dominates with respect to h. The simulated flows between groundwater and surface water bodies (Q_{swb}) are clearly most sensitive to R. This is due to the model parameterization of river conductance that is

10   computed as a function of R, assuming under steady-state conditions, groundwater discharge to rivers should tend to increase with increasing R (Eq. (3)). The results indicate that changes in R between timesteps for a fully coupled transient model could pose a challenge to the model convergence and that the equations might need to be reconsidered for a fully coupled model. In general the uncertainty due to the parameterization of groundwater-surface water exchange flows (E_{swb} and $C_{riv,gl.wet,wet,lak}$) needs to be further investigated as they have a high impact on h distribution and Q_{swb}.

15   In high mountainous regions (Rocky Mountains, Andes, Ethiopian Highlands, Arabian Peninsula, Himalaya) and regions with low recharge (Sahara, southern Africa) the computed h showed an unreasonably high variance due to the numeric instability of the simulations in these areas. In case of high elevations and thus large variations in E_{swb} or in case of low groundwater recharge, it is not possible to solve steady-state groundwater flow equations with arbitrary parameter combinations and a constant convergence parameter. Q_{swb} was found to somewhat be more robust than h in these regions. These results suggest that

20   the parameterization of E_{swb} needs to be reconsidered and is a likely parameter for future calibration.

The lack of reliable data at the global scale, in particular hydraulic conductivity data with high horizontal and vertical resolution, hinders the development of global groundwater models. A simple sensitivity analysis on the impact of small changes to an existing global hydraulic conductivity dataset (GLHYMPS 1.0 (Gleeson et al., 2014) to 2.0 (Huscroft et al., 2018)) showed that knowledge about the distribution of K is pivotal for the simulation of h as even slight changes in K may change model

25   results by up to 100 m.

The presented study results refer to the uncoupled steady-state groundwater model G^{3}M. As G^{3}M is currently being integrated into the global hydrological model WaterGAP, future work will extend this sensitivity analysis to fully coupled transient simulations.

1   Appendix

30   Results of the method of Morris need to be contemplated in a ranking based scheme that relies on metrics that summarize the calculated EEs. Figure A1 shows the conceptual issues that are entailed with this ranking approach. The absolute mean ($\mu*$) of all EEs of parameter 1 (P1) might be bigger than $\mu*$ of P2 but as their CIs are overlapping a clear ranking is not possible. On the other hand it is evident that P1 and P2 are clearly more sensitive than P3. Figure A2 shows regions where the applied sampling
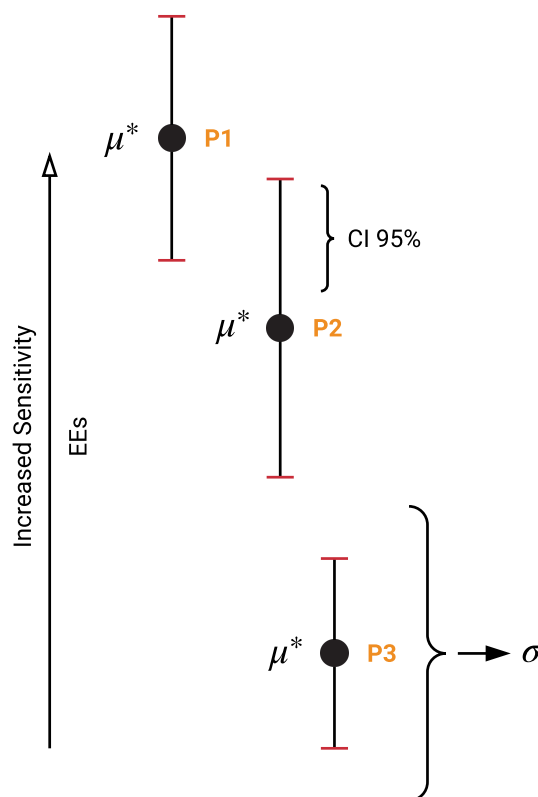
Figure A1. Illustration of derivation of presented metrics.

was sufficient (CIs where smaller than 15% of the calculated $\mu*$ of the first rank) and regions where more simulations, or a more sophisticated approach to ensure numerical stability, is required.

Author contributions. RR led conceptualization, formal analysis, methodology, software, visualization, and writing of the original draft. JH, LF, SM, TT supported review and editing as well as the development of the methodology. AW supported visualization and writing of the original draft. PD supervised the work of RR and made suggestions regarding analysis, structure, and wording of the text and design of tables and figures.

Acknowledgements. Funding: Friedrich-Ebert Foundation PhD fellowship
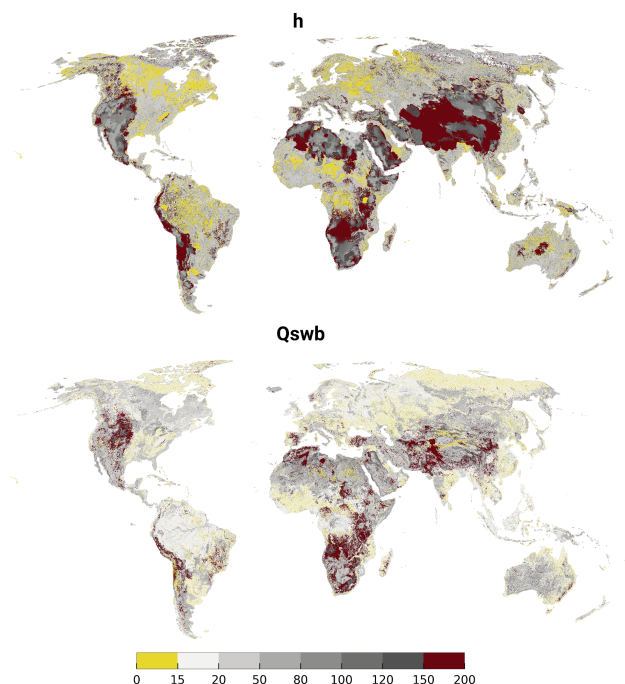
Figure A2. Confidence interval (95) in relation to the $\mu*$ for rank 1 of h and Q_{swb}. Yellow regions indicate a sufficient sampling size.

References

Allen, P. M., Arnold, J. C., and Byars, B. W.: Downstream channel geometry for use in planning-level models, JAWRA Journal of the American Water Resources Association, 30, 663–671, https://doi.org/10.1111/j.1752-1688.1994.tb03321.x, 1994.

Archer, G., Saltelli, A., and Sobol, I.: Sensitivity measures, ANOVA-like techniques and the use of bootstrap, Journal of Statistical Computation and Simulation, 58, 99–120, 1997.

Börker, J., Hartmann, J., Amann, T., and Romero-Mujalli, G.: Global Unconsolidated Sediments Map Database v1.0 (shapefile and gridded to 0.5° spatial resolution), https://doi.org/10.1594/PANGAEA.884822, supplement to: Börker, J et al. (accepted): Terrestrial Sediments of the Earth: Development of a Global Unconsolidated Sediments Map Database (GUM). Geochemistry, Geophysics, Geosystems, https://doi.org/10.1002/2017GC007273, 2018.

Branger, F., Giraudet, L.-G., Guivarch, C., and Quirion, P.: Global sensitivity analysis of an energy–economy model of the residential building sector, Environmental Modelling & Software, 70, 45 – 54, https://doi.org/https://doi.org/10.1016/j.envsoft.2015.03.021, 2015.

Campolongo, F., Cariboni, J., and Saltelli, A.: An effective screening design for sensitivity analysis of large models, Environmental modelling & software, 22, 1509–1518, https://doi.org/10.1016/j.envsoft.2006.10.004, 2007.

Cariboni, J., Gatelli, D., Liska, R., and Saltelli, A.: The role of sensitivity analysis in ecological modelling, Ecological Modelling, 203, 167 – 182, https://doi.org/10.1016/j.ecolmodel.2005.10.045, special Issue on Ecological Informatics: Biologically-Inspired Machine Learning, 2007.

Chaney, N., Herman, J., Reed, P., and Wood, E.: Flood and drought hydrologic monitoring: the role of model parameter uncertainty, Hydrology and Earth System Sciences, 19, 3239–3251, https://doi.org/10.5194/hess-19-3239-2015, 2015.

de Graaf, I. E., Sutanudjaja, E., Van Beek, L., and Bierkens, M.: A high-resolution global-scale groundwater model, Hydrology and Earth System Sciences, 19, 823–837, https://doi.org/10.5194/hess-19-823-2015, 2015.

5 de Graaf, I. E., van Beek, R. L., Gleeson, T., Moosdorf, N., Schmitz, O., Sutanudjaja, E. H., and Bierkens, M. F.: A global-scale two-layer transient groundwater model: Development and application to groundwater depletion, Advances in Water Resources, 102, 53–67, https://doi.org/10.1016/j.advwatres.2017.01.011, 2017.

Döll, P., Kaspar, F., and Lehner, B.: A global hydrological model for deriving water availability indicators: model tuning and validation, Journal of Hydrology, 270, 105–134, https://doi.org/10.1016/S0022-1694(02)00283-4, 2003.

10 Döll, P., Hoffmann-Dobrev, H., Portmann, F. T., Siebert, S., Eicker, A., Rodell, M., Strassberg, G., and Scanlon, B.: Impact of water withdrawals from groundwater and surface water on continental water storage variations, Journal of Geodynamics, 59, 143–156, https://doi.org/10.1016/j.jog.2011.05.001, 2012.

Döll, P., Müller Schmied, H., Schuh, C., Portmann, F. T., and Eicker, A.: Global-scale assessment of groundwater depletion and related groundwater abstractions: Combining hydrological modeling with information from well observations and GRACE satellites, Water Re-
15 sources Research, 50, 5698–5720, https://doi.org/10.1002/2014WR015595, 2014.

Fan, Y., Li, H., and Miguez-Macho, G.: Global patterns of groundwater table depth, Science, 339, 940–943, https://doi.org/10.1126/science.1229881, 2013.

Ghasemizade, M., Baroni, G., Abbaspour, K., and Schirmer, M.: Combined analysis of time-varying sensitivity and identifiability indices to diagnose the response of a complex environmental model, Environmental Modelling & Software, 88, 22 – 34,
20 https://doi.org/10.1016/j.envsoft.2016.10.011, 2017.

Gleeson, T., Smith, L., Moosdorf, N., Hartmann, J., Dürr, H. H., Manning, A. H., van Beek, L. P. H., and Jellinek, A. M.: Mapping permeability over the surface of the Earth, Geophysical Research Letters, 38, https://doi.org/10.1029/2010GL045565, 2011.

Gleeson, T., Moosdorf, N., Hartmann, J., and Van Beek, L.: A glimpse beneath earth's surface: GLobal HYdrogeology MaPS (GLHYMPS) of permeability and porosity, Geophysical Research Letters, 41, 3891–3898, https://doi.org/10.1002/2014GL059856, 2014.

25 Gruber, S.: Derivation and analysis of a high-resolution estimate of global permafrost zonation, The Cryosphere, 6, 221–233, https://doi.org/10.5194/tc-6-221-2012, 2012.

Hartmann, J. and Moosdorf, N.: Global Lithological Map Database v1.0 (gridded to 0.5° spatial resolution), https://doi.org/10.1594/PANGAEA.788537, 2012.

Hengl, T., Mendes de Jesus, J., Heuvelink, G. B. M., Ruiperez Gonzalez, M., Kilibarda, M., Blagotić, A., Shangguan, W., Wright, M. N.,
30 Geng, X., Bauer-Marschallinger, B., Guevara, M. A., Vargas, R., MacMillan, R. A., Batjes, N. H., Leenaars, J. G. B., Ribeiro, E., Wheeler, I., Mantel, S., and Kempen, B.: SoilGrids250m: Global gridded soil information based on machine learning, PLOS ONE, 12, 1–40, https://doi.org/10.1371/journal.pone.0169748, 2017.

Herman, J. and Usher, W.: SALib: an open-source Python library for sensitivity analysis, The Journal of Open Source Software, 2, https://doi.org/10.21105/joss.00097, 2017.

35 Herman, J., Kollat, J., Reed, P., and Wagener, T.: Method of Morris effectively reduces the computational demands of global sensitivity analysis for distributed watershed models, Hydrology and Earth System Sciences, 17, 2893–2903, https://doi.org/10.5194/hess-17-2893-2013, 2013a.

Herman, J. D., Reed, P. M., and Wagener, T.: Time-varying sensitivity analysis clarifies the effects of watershed model formulation on model behavior, Water Resources Research, 49, 1400–1414, https://doi.org/10.1002/wrcr.20124, 2013b.

Huscroft, J., Gleeson, T., Hartmann, J., and Börker, J.: Compiling and mapping global permeability of the unconsolidated and consolidated Earth: GLobal HYdrogeology MaPS 2.0 (GLHYMPS 2.0), Geophysical Research Letters, 45, 1897–1904, https://doi.org/10.1002/2017GL075860, 2018.

Keune, J., Gasper, F., Goergen, K., Hense, A., Shrestha, P., Sulis, M., and Kollet, S.: Studying the influence of groundwater representations on land surface-atmosphere feedbacks during the European heat wave in 2003, Journal of Geophysical Research: Atmospheres, 121, 13,301–13,325, https://doi.org/10.1002/2016JD025426, 2016.

Koirala, S., Kim, H., Hirabayashi, Y., Kanae, S., and Oki, T.: Sensitivity of global hydrological simulations to groundwater capillary flux parameterizations, Water Resources Research, 54, https://doi.org/10.1029/2018WR023434, 2018.

Konikow, L. F.: Contribution of global groundwater depletion since 1900 to sea-level rise, Geophysical Research Letters, 38, https://doi.org/10.1029/2011GL048604, 2011.

Lloyd, S.: Least squares quantization in PCM, IEEE Transactions on Information Theory, 28, 129–137, https://doi.org/10.1109/TIT.1982.1056489, 1982.

Maxwell, R. M., Condon, L. E., and Kollet, S. J.: A high-resolution simulation of groundwater and surface water over most of the continental US with the integrated hydrologic model ParFlow v3, Geoscientific Model Development, 8, 923–937, https://doi.org/10.5194/gmd-8-923-2015, 2015.

Miguez-Macho, G., Fan, Y., Weaver, C. P., Walko, R., and Robock, A.: Incorporating water table dynamics in climate modeling: 2. Formulation, validation, and soil moisture simulation, Journal of Geophysical Research: Atmospheres, 112, https://doi.org/10.1029/2006JD008112, 2007.

Morel-Seytoux, H. J., Miller, C. D., Miracapillo, C., and Mehl, S.: River Seepage Conductance in Large-Scale Regional Studies, Groundwater, 55, 399–407, https://doi.org/10.1111/gwat.12491, 2017.

Morris, M. D.: Factorial sampling plans for preliminary computational experiments, Technometrics, 33, 161–174, https://doi.org/10.1080/00401706.1991.10484804, 1991.

Müller Schmied, H., Eisner, S., Franz, D., Wattenbach, M., Portmann, F. T., Flörke, M., and Döll, P.: Sensitivity of simulated global-scale freshwater fluxes and storages to input data, hydrological model structure, human water use and calibration, Hydrology and Earth System Sciences, 18, 3511–3538, https://doi.org/10.5194/hess-18-3511-2014, 2014.

Müller Schmied, H., Adam, L., Eisner, S., Fink, G., Flörke, M., Kim, H., Oki, T., Portmann, F. T., Reinecke, R., Riedel, C., et al.: Variations of global and continental water balance components as impacted by climate forcing uncertainty and human water use, Hydrology and Earth System Sciences, 20, 2877–2898, https://doi.org/10.5194/hess-20-2877-2016, 2016.

Pianosi, F., Beven, K., Freer, J., Hall, J. W., Rougier, J., Stephenson, D. B., and Wagener, T.: Sensitivity analysis of environmental models: A systematic review with practical workflow, Environmental Modelling & Software, 79, 214–232, https://doi.org/10.1016/j.envsoft.2016.02.008, 2016.

Reinecke, R.: G^{3}M-f a global gradient-based groundwater modelling framework, JOSS, 3, 548, https://doi.org/10.21105/joss.00548, 2018.

Reinecke, R., Foglia, L., Mehl, S., Trautmann, T., Cáceres, D., and Döll, P.: Beyond the bucket – Developing a global gradient-based groundwater model (G^{3}M v1.0) for a global hydrological model from scratch, Geoscientific Model Development Discussions, 2018, 1–21, https://doi.org/10.5194/gmd-2018-120, 2018.

Ruano, M., Ribes, J., Seco, A., and Ferrer, J.: An improved sampling strategy based on trajectory design for application of the Morris method to systems with many input factors, Environmental Modelling & Software, 37, 103 – 109, https://doi.org/10.1016/j.envsoft.2012.03.008, 2012.

Saltelli, A., Ratto, M., Andres, T., Campolongo, F., Cariboni, J., Gatelli, D., Saisana, M., and Tarantola, S.: Global sensitivity analysis: the primer, John Wiley & Sons, 2008.

Scanlon, B. R., Faunt, C. C., Longuevergne, L., Reedy, R. C., Alley, W. M., McGuire, V. L., and McMahon, P. B.: Groundwater depletion and sustainability of irrigation in the US High Plains and Central Valley, Proceedings of the National Academy of Sciences, 109, 9320–9325, https://doi.org/10.1073/pnas.1200311109, 2012.

Schumacher, M., Eicker, A., Kusche, J., Schmied, H. M., and Döll, P.: Covariance analysis and sensitivity studies for GRACE assimilation into WGHM, in: IAG 150 Years, pp. 241–247, Springer, https://doi.org/10.1007/1345_2015_119, 2015.

Sobol, I. M.: Sensitivity estimates for nonlinear mathematical models, Mathematical Modelling and Computational Experiments, 1, 407–414, 1993.

Song, X., Zhang, J., Zhan, C., Xuan, Y., Ye, M., and Xu, C.: Global sensitivity analysis in hydrological modeling: Review of concepts, methods, theoretical framework, and applications, Journal of Hydrology, 523, 739 – 757, https://doi.org/10.1016/j.jhydrol.2015.02.013, 2015.

Stonestrom, D. A.: Ground-water recharge in the arid and semiarid southwestern United States, 1703, USGS, http://pubs.usgs.gov/pp/pp1703, 2007.

Taylor, R. G., Scanlon, B., Döll, P., Rodell, M., Van Beek, R., Wada, Y., Longuevergne, L., Leblanc, M., Famiglietti, J. S., Edmunds, M., et al.: Ground water and climate change, Nature Climate Change, 3, 322, https://doi.org/10.1038/nclimate1744, 2013.

Verzano, K., Bärlund, I., Flörke, M., Lehner, B., Kynast, E., Voß, F., and Alcamo, J.: Modeling variable river flow velocity on continental scale: Current situation and climate change impacts in Europe, Journal of hydrology, 424, 238–251, https://doi.org/10.1016/j.jhydrol.2012.01.005, 2012.

Wada, Y.: Modeling Groundwater Depletion at Regional and Global Scales: Present State and Future Prospects, Surveys in Geophysics, 37, 419–451, https://doi.org/10.1007/s10712-015-9347-x, 2016.

Wada, Y., Beek, L. P. H., and Bierkens, M. F. P.: Nonsustainable groundwater sustaining irrigation: A global assessment, Water Resources Research, 48, https://doi.org/10.1029/2011WR010562, 2012.

Wada, Y., Wisser, D., and Bierkens, M. F. P.: Global modeling of withdrawal, allocation and consumptive use of surface water and groundwater resources, Earth System Dynamics, 5, 15–40, https://doi.org/10.5194/esd-5-15-2014, 2014.

Zhan, C., meng Song, X., Xia, J., and Tong, C.: An efficient integrated approach for global sensitivity analysis of hydrological model parameters, Environmental Modelling & Software, 41, 39 – 52, https://doi.org/10.1016/j.envsoft.2012.10.009, 2013.